Title

Mechanistic Development of CPT-Based Cyclic Strength Correlations for Clean Sand

Journal

Journal of Geotechnical and Geoenvironmental Engineering, 145(10)

ISSN

1090-0241

Authors

Moug, Diane M
Price, Adam B
Bastidas, Ana Maria Parra
et al.

Publication Date

2019-10-01

DOI

10.1061/(asce)gt.1943-5606.0002101

Peer reviewed

Title: Mechanistic Development of CPT-based Cyclic Strength Correlations for a Clean Sand
Submission to: ASCE Journal of Geotechnical and Geoenvironmental Engineering
Article Type: Technical Paper
Authors' copy: Final manuscript, June 2019, before copyediting and publication

---

Author 1
- Diane M. Moug, Ph.D., A.M. ASCE
- Assistant Professor; Department of Civil and Environmental Engineering, Portland State University, Portland, OR, 95701, dmoug@pdx.edu.

Author 2
- Adam B. Price, Ph.D., M. ASCE
- Senior Staff Engineer; Fugro USA Land, Inc., Walnut Creek, CA, USA, a.price@fugro.com.

Author 3
- Ana Maria Parra Bastidas, Ph.D., E.I.T., M. ASCE
- Projects Engineer; Carlos H. Parra & Associates, Cali, Colombia, 760008, aparrabastidas@ucdavis.edu.

Author 4
- Kathleen M. Darby, Ph.D., S.M. ASCE
- Senior Staff Engineer; Geosyntec Consultants, Oakland, CA, 94612, kdarby@ucdavis.edu.

Author 5
- Ross W. Boulanger, Ph.D., P.E., F. ASCE
- Professor; Department of Civil and Environmental Engineering, University of California, Davis, CA, 95616, rwboulanger@ucdavis.edu.

Author 6
- Jason T. DeJong, Ph.D., M. ASCE
- Professor; Department of Civil and Environmental Engineering, University of California, Davis, CA, 95616, jdejong@ucdavis.edu.

Mechanistic Development of CPT-based Cyclic Strength Correlations for a Clean Sand

Abstract

Mechanistic approaches for developing cone penetration test-based liquefaction triggering correlations are presented and evaluated with an application to Ottawa sand. The mechanistic approaches utilize combinations of data from: undrained cyclic direct simple shear tests, dynamic geotechnical centrifuge tests with in-flight cone penetration profiles, and cone penetration simulations. Cyclic direct simple shear tests on Ottawa sand characterize the relationship between cyclic resistance ratio (CRR) and relative density (D_R). Relationships between cone tip resistance (q_c) and D_R are developed from geotechnical centrifuge tests and cone penetration simulations. Penetration simulations using the MIT-S1 constitutive model with three different calibrations for Ottawa sand examine the role of critical state line shape and position on simulated q_c values. The $CRR - D_R$ relationship from laboratory tests is composed with measured and simulated $q_C - D_R$ relationships via common $D_R$values to develop $CRR - q_c$ relationships. An alternative $CRR - q_c$ relationship is developed from inverse analyses of centrifuge test sensor array data (i.e., arrays of accelerometers and pore pressure sensors). The results of these different approaches are compared to case history-based correlations for clean sand and their relative merits discussed. Recommendations are provided for future application of these mechanistic approaches for developing liquefaction triggering correlations of poorly characterized or unique soils.

Introduction

A liquefaction triggering relationship for cyclic resistance ratio (CRR) from the cone penetration tip resistance (q_c) for clean silica sand is reasonably well established from case history-based semi-empirical correlations (e.g., Boulanger and Idriss 2016, Robertson and Wride 1998, Youd et al. 2001). These correlations were developed from earthquake case histories where site observations indicated that liquefaction triggering or no-triggering occurred (e.g., presence or absence of lateral spreading, sand boils, building settlement) and cone penetration test (CPT) measurements were available. Early $CRR - q_c$ liquefaction triggering correlations, such as Robertson and Campanella (1985), or Seed and De Alba (1986), were based on $CRR - N$ correlations where the Standard Penetration Test (SPT) N value was converted to an equivalent q_c value. The number of clean sand liquefaction or no-liquefaction sites characterized with CPT q_c profiles and summarized in case history databases (i.e., Boulanger and Idriss 2014, Moss et al. 2003) later became sufficient to develop $CRR - q_c$ triggering correlations directly from measured q_c values.

Soils that are susceptible to liquefaction yet not well represented in the case history database include soils intermediate to sands and clays (e.g., non-plastic silt, silty sand, clayey silt) and non-silica soils. Consequently, these soils do not have well developed engineering relationships for estimating their liquefaction resistance or cyclic strength.

In addition to case history-based methods, $CRR - q_c$ liquefaction triggering relationships have also been developed mechanistically by various approaches. Mitchell and Tseng (1990) developed triggering relationships for four different sands by combining the CRR from laboratory tests and q_c from cavity expansion simulations through the sand relative density (D_R). The relationships were independently evaluated with laboratory testing on undisturbed field samples

from sites where q_c profiles were measured. Carraro et al. (2003) developed $CRR - q_c$ relationships for clean and silty sands with cyclic triaxial tests and cylindrical cavity expansion simulations; the developed relationships were compared to case history-based correlations for the appropriate range of fines contents. Kokusho et al. (2006) directly developed $CRR - q_c$ curves for sand with varying fines content by preparing specimens in a cyclic triaxial apparatus and measuring q_c with a mini cone penetrometer before the specimens were cyclically loaded.

This paper evaluates mechanistic approaches for synthesizing data from laboratory testing, geotechnical centrifuge testing, and numerical simulations of cone penetration to develop $CRR - q_c$ relationships for clean Ottawa F-65 sand ("Ottawa sand"). A framework for relating the various components of these approaches is depicted in Fig. 1. These framework components, how they are interrelated, and how they are combined are discussed in the following sections of this paper:

- *Laboratory characterization of Ottawa sand* (Parra Bastidas 2016). Monotonic laboratory tests inform the calibration of the constitutive model used in the cone penetration simulations. Cyclic direct simple shear (DSS) tests are used to develop a $CRR - D_R$ relationship.
- *Geotechnical centrifuge testing* (Darby et al. 2016, 2017, 2019a). Centrifuge tests of level uniform soil profiles with multiple shaking events provide data for evaluating CRR and q_c values for progressively increasing D_R values. In-flight cone penetration tests provide $q_c - D_R$ data that inform calibration and validation of the cone penetration simulations. Inverse analyses of sensor array data for each shaking event provide $CSR - q_c$ points for liquefaction/no-liquefaction observations as well as $CRR - q_c$ points based on the time of liquefaction triggering.

- *Cone penetration simulations*. Numerical simulations with a direct penetration model in the finite difference program FLAC (Fast Lagrangian Analysis of Continua; Itasca 2016) with the MIT-S1 constitutive model provide $q_c - D_R$ relationships and q_c stress normalization relationships. Three different calibrations of the MIT-S1 model provide insight into the soil behaviors and model parameters that most influence penetration resistance.
- *Development of $CRR - q_c$ relationships*. The $CRR - D_R$ relationship from laboratory testing is composed with each of the three alternative $D_R - q_c$ relationships from the numerical simulations to produce three composite relationships for $CRR - q_c$. Two more, largely independent, $CRR - q_c$ relationships are provided by composing the $CRR - D_R$ relationship from laboratory testing with the $D_R - q_c$ relationship from the in-flight cone penetration tests, and plotting the CRR from inverse analyses of the centrifuge sensor arrays directly against the in-flight q_c data. Comparison of the above $CRR - q_c$ relationships with case history-based correlations provide a basis for evaluating their consistency.

The results of this study using Ottawa sand provide a basis for discussing the relative merits of alternative approaches to mechanistically developing $CRR - q_c$ relationships, the challenges involved in each component of these approaches, and the consistency of the results with case history-based correlations for a soil type that is relatively well understood. Recommendations are provided for future application of the mechanistic framework for developing liquefaction triggering correlations of poorly characterized or unique soils.

Laboratory Characterization of Ottawa Sand

Ottawa F-65 sand is a quartzitic, uniform, rounded sand that is mined by U.S. Silica Corp. from St. Peter sandstone deposits near Ottawa, Illinois. Characterization of this sand by Parra

Bastidas et al. (2016) includes: (1) the index properties summarized in Table 1, (2) one-dimensional (1-D) compression and monotonic undrained DSS tests to support calibration of the soil constitutive model for penetration simulations, and (3) cyclic undrained DSS tests to characterize the relationship between CRR and D_R. Experimental procedures, equipment, and specimen preparation are detailed in Parra Bastidas (2016).

Monotonic Properties for Modeling Cone Penetration

1-D compression tests were performed on dry funnel deposited and air pluviated specimens of Ottawa sand that were initially consolidated to a vertical effective consolidation stress (σ'_{vc}) of 100 kPa. The results of tests on initially loose (void ratio, e, = 0.727) and initially dense (e = 0.536) specimens are presented in Fig. 2. The loading path for both tests transition onto the Limiting Compression Curve (LCC) at high compressive stresses where the compression behavior is independent of initial specimen preparation and the primary mechanisms of void ratio change are particle crushing and particle rearrangements (Pestana and Whittle 1995). The loose specimen transitions onto the LCC at a mean effective stress (p') of about 30 MPa, and the dense specimen transitions onto the LCC at about p' = 50 MPa. A linear LCC in log(p')-log(e) space, is indicated by the dashed line in Fig. 2.

Undrained monotonic DSS tests were performed on saturated, normally consolidated specimens. The stress-strain and stress path responses for representative specimens are shown in Fig. 3. Specimens were prepared at initial D_R = 29%-32% (will be referred to as 30%), and 73%-75% (will be referred to as 75%), and σ'_{vc} = 100, 400, and 800 kPa.

Cyclic Strengths from Direct Simple Shear Testing

Undrained cyclic DSS tests were performed on specimens for two conditions: virgin, normally consolidated specimens, and specimens subjected to multiple cyclic loading and reconsolidation stages. Virgin specimens characterize the relationship between the cyclic stress ratio ($CSR = \tau/\sigma'_{vc}$) and number of uniform loading cycles (N_{cyc}) to reach 3% maximum shear strain (γ_{max}). Specimens that were repeatedly cyclically loaded and reconsolidated characterized the increase in cyclic resistance ratio (CRR) with increasing D_R. The CRR is defined herein, unless otherwise noted, as the CSR required to achieve γ_{max} = 3% in 15 cycles of loading (i.e., $CRR_{N=15,\gamma_{max}=3\%}$). Note that an excess pore pressure ratio ($r_u = \Delta u/\sigma'_{vc}$) of 1.0 is strongly correlated with the development of γ_{max} of 2 to 3%.

Virgin specimens for cyclic loading were prepared at D_R = 40% ("loose") and D_R = 80% ("dense") and tested at σ'_{vc} = 50, 100, and 400 kPa. The CSR versus N_{cyc} to reach γ_{max} = 3% is shown in Fig. 4. The data are fit with the regression:

$$CSR = a \cdot N^{-b} \quad (1)$$

where a and b are fitting parameters (Idriss and Boulanger, 2008). Regressions for the σ'_{vc} = 100 kPa specimens have b values of 0.15 and 0.17 for D_R = 40% and 80%, respectively. The curves for the σ'_{vc} = 50 kPa, and 400 kPa data were assumed to parallel the σ'_{vc} = 100 kPa curves, and therefore were fit with the same respective b values. A b = 0.15 value is used to project $CRR_{N=15}$ for the cyclic DSS tests described herein. These b values are within the range of published values for clean loose sand as summarized in Boulanger and Idriss (2014) or Parra Bastidas (2016).

Specimens subject to multiple cyclic loading stages were re-centered and reconsolidated to σ'_{vc} = 100 kPa under zero shear strain conditions following each cyclic loading stage. The CSR was increased in the loading sequence when more than 100 cycles of loading were required to reach γ_{max} = 3%. Equivalent values for $CRR_{N=15}$ were projected based on the b value reported above, and are summarized in Fig. 5 for γ_{max} = 1% and 3%. To facilitate comparing the $CRR - q_c$ relationships developed from these laboratory CRR values (which involve one-directional cyclic loading) to any case history-based correlation, a correction must be applied to obtain equivalent values for the multi-directional shaking conditions encountered in the field. Therefore, the $CRR_{N=15}$ values in Fig. 5 are presented with a 10% reduction to account for bi-directional shaking effects per the recommendations of Seed (1979). The data were fit with relationships for $CRR_{N=15,\gamma_{max}=1\%} - D_R$ and $CRR_{N=15,\gamma_{max}=3\%} - D_R$, which show that the failure criterion had a progressively larger effect on CRR as the specimen density increased. The relationship for $CRR_{N=15,\gamma_{max}=3\%}$ is used later to develop composite liquefaction triggering relationships.

Geotechnical Centrifuge Testing

Three geotechnical centrifuge tests of Ottawa sand models were performed on the 9 m radius centrifuge at the UC Davis Center for Geotechnical Modeling. All tests were performed at a centrifugal acceleration of 40 g; results are presented in prototype scale using standard dynamic scaling laws unless otherwise noted. The centrifuge models are referenced as KMD01, KMD02, and KMD03. Experimental details are provided in Darby et al. (2016, 2017, 2019a).

The three models had a uniform 10 m thick layer of Ottawa sand with a level surface, underlain by a 7.2 m thick layer of dense Monterrey sand. The sands were deposited by air pluviation where the D_R was controlled by the drop height and mesh size at the base of the sand

pluviator. The Ottawa sand was prepared at $D_R \approx 43\%$ for KMD01, $D_R \approx 25\%$ for KMD02, and $D_R \approx 80\%$ for KMD03. The Monterey sand was prepared at $D_R \approx 85\%$ for all three models. Model instrumentation in the Ottawa sand unit included two vertical arrays of eleven pore pressure transducers (PPTs), two vertical arrays of eleven accelerometers, and four linear potentiometers (LPs) located at the model surface.

Each model was subjected to a series of sinusoidal shaking events with cone penetration tests before or after select shaking events. The timelines for shaking events and cone penetration soundings for each experiment are illustrated versus shaking event number in Fig. 6. The sinusoidal shaking events had 15 uniform cycles of base acceleration at a frequency of 1.0 Hz. The symbols plotted in Fig. 6 indicate the peak base acceleration (PBA) applied to the model (left y-axis) and the maximum excess pore pressure ratio (indicated by symbol shade) measured by a PPT at different depths (indicated by symbol shape) for each shaking event. The r_u values are presented in these figures for greater than 0.95 (dark symbols), between 0.70 and 0.95 (light symbols), or less than 0.70 (no fill). The depths for these r_u measurements approximately ranged from 2.7 m to 7.5 m, as indicated by the symbol shape. The gray filled line in Fig. 6 indicates the average volumetric strain (right y-axis) that was estimated by LP measurements for each shaking event.

Cone Penetration Testing

Cone penetrometer profiles were obtained before the model was subjected to shaking and after select shaking series. The cone penetrometer had a 6 mm diameter (model units) and was pushed at approximately 1 cm/second by a hydraulic actuator, which is sufficiently slow to ensure fully drained conditions during penetration in these sands. To re-position the CPT actuator, the centrifuge was spun down and spun up between shaking series; the influence of starting and stopping the centrifuge to re-position the cone was shown to have no measureable effect on q_c

values (Darby et al. 2017). The point in the testing sequence that the cone was pushed is shown on the top x-axes on Fig. 6. The cone was pushed 8 times during KMD01 and KMD02, and 11 times in KMD03.

Measured cone penetration resistance profiles are shown in Fig. 7 for KMD01, KMD02, and KMD03; the depth is referenced from the original model surface. These profiles show that the q_c values progressively increased as the model densified over the course of multiple shaking events. For shaking events where the cone was not pushed, q_c values were linearly interpolated based on the measured settlements for events between cone pushes. Overburden corrected penetration resistances were computed as $q_{c1N} = C_N q_c / P_a$ (where P_a is atmospheric pressure) using the C_N relationship by Idriss and Boulanger (2008) with the model specific $D_R - q_c$ correlation by Darby et al. (2017).

Cyclic Strengths from Inverse Analysis

CRR values at different depths were computed from inverse analyses of the accelerometer and PPT array data following the procedures described in Darby et al. (2019a). Liquefaction triggering for these level ground conditions was evaluated based on the peak r_u during shaking; a peak value of 1.0 indicates that the soil's effective stress temporarily dropped to zero and "liquefaction" was triggered. The r_u criteria for liquefaction triggering was relaxed to 0.95 to account for uncertainties in test measurements. Time series of CSR were computed by integration of mass times acceleration along the vertical accelerometer arrays assuming 1-D wave propagation, using the procedures described in Kamai and Boulanger (2010). These CSR time series were converted to an equivalent 15 uniform loading cycles time series using the fatigue-based procedure by Seed et al. (1975) with a b value of 0.20. This b value was found to reasonably

interpret dynamic centrifuge test results through a sensitivity analysis, and falls into the range reported in Parra Bastidas (2016) and in Ziotopoulou et al. (2018) for cyclic DSS tests on Ottawa sand. CRR values were similarly determined by converting the CSR time series up to liquefaction triggering to an equivalent CRR value for 15 uniform loading cycles. Both CRR and CSR values are further adjusted to account for the effects of overburden, bi-directional shaking, and partial drainage during loading; these adjustments are described in detail in Darby et al. (2019a,b).

Each shaking event from KMD01, KMD02, and KMD03 is plotted with the corresponding CSR (for non-triggering events; open symbols) or CRR (for triggering events; filled symbols) versus q_{c1N} in Fig. 8. The CRR values are labelled as either medium confidence (triangles) or high confidence (diamonds) based on their sensitivity to various measurement uncertainties as detailed in Darby et al. (2019a). The centrifuge test data include points with extremely large CSR values (in the range of 1.0 to 2.2), which greatly exceed the loading levels represented in liquefaction case history databases. The case history-based correlation for CRR by Boulanger and Idriss (2016) is also plotted on Fig. 8 with the shaded area representing the plus or minus one standard deviation range in estimated CRR values. The Boulanger and Idriss (2016) relationship was based on case histories with CSR values less than about 0.60, and thus extension of this relationship to larger CRR values requires extrapolating outside case history observations. The comparison shown in Fig. 8 indicates reasonable agreement between the case history-based correlation and the results of the dynamic centrifuge model experiments.

Cone Penetration Simulations

An axisymmetric cone penetration model was used to simulate cone penetration in Ottawa sand, from which a $q_c - D_R$ relationship and its dependence on overburden stress was developed.

The simulations were performed using the explicit finite difference program FLAC (Fast Lagrangian Analysis of Continua; Itasca 2016) with the MIT-S1 constitutive model (Pestana and Whittle 1999, 2002a,b) calibrated for Ottawa sand. Penetration was simulated with three different calibrations for the MIT-S1 model to evaluate the soil properties and model parameters that strongly affect cone penetration resistance.

Cone Penetration Model

The axisymmetric model geometry simulates steady-state penetration at one depth in the soil column for a standard 10 cm^2 (3.568 cm diameter) cone as shown in Fig. 9. The model is initialized with stress and material properties for the "wished-in-place" condition at the depth of interest in the soil column. Cone geometry and conditions between the cone and soil are captured with Mohr-Coulomb interface elements that obey the Mohr-Coulomb friction condition. The boundary conditions are specified for soil flowing upwards relative to a stationary cone; soil conceptually flows into the bottom of the model and exits at the top of the model. The in-situ vertical stress is applied across the bottom boundary, where this boundary is sufficiently far from the penetrating cone's zone of influence that the in-situ stress condition prevails. The right radial boundary is represented with an infinite elastic boundary condition and is sufficiently far from the penetrating cone to avoid boundary effects. The cone penetration velocity is applied to all gridpoints across the top boundary. Penetration is then simulated until steady state penetration resistance is reached. Large deformations are addressed with a user-implemented ALE algorithm that performs rezoning and remapping operations throughout simulated penetration (Moug et al. 2019).

The interface coefficient of friction ($\delta = \phi_{cone}/\phi_{critical\ state}$) was set at 0.6, where 0.0 would represent a perfectly smooth cone and 1.0 would represent a perfectly rough cone. The work of Uesugi and Kishida (1986) examined the coefficient of friction between sand-steel interfaces

and showed that δ increases linearly from 0.4 to 0.8 for smooth to rough steel surfaces, which approximately correspond to the surfaces of new and heavily used cone tips and sleeves, respectively. Therefore, a δ value of 0.6 was specified to represent friction along the cone tip and shaft. The stiffness of the shear and normal springs in these interface elements were set large enough that they had negligible effects on the solution (Itasca 2016), which was confirmed by sensitivity analyses.

Initial stress conditions all corresponded to a normally consolidated K_o (coefficient of lateral earth pressure at rest) condition. Fully drained penetration conditions were imposed by setting the pore water bulk modulus to a small value; simulation results confirmed negligible pore pressure was generated during penetration.

MIT-S1 Constitutive Model Calibration

The MIT-S1 constitutive model is a bounding surface plasticity model that is capable of capturing soil behavior from sedimentary clays to clean sands (Pestana and Whittle 1999, 2002a,b). The version of MIT-S1 used in this study was initially implemented by Jaeger (2012) who made some minor modifications to the model. Additional modifications to the MIT-S1 implementation for the penetration model in FLAC are described in Moug (2017).

Calibration of MIT-S1 was informed by well-established empirical correlations and the laboratory test data described previously, but the selection of certain key parameters remained subjective. For this reason, three different calibrations were developed; Table 2 lists the different model parameters, their primary purposes, and their assigned values for the three calibrations. For brevity, the following discussion focuses on how the different calibrations influence different features of simulated stress-strain responses. A detailed description of each model parameter and the basis for its selection is detailed in Moug (2017) and Price (2017).

The three calibrations are consistent in their representation, demonstrated through single-element simulations, of: (a) measured 1-D compression behavior at high stresses, as shown in Fig. 10b and discussed later, (b) small strain shear modulus (G_{max}) and shear modulus reduction with shear strain ($G/G_{max} - \gamma$) as shown in Fig. 11, and (c) stress-dilatancy relations as shown in Fig. 12. These features of model behavior are consistent because thirteen of the sixteen model parameters listed in Table 2 have the same value for the three calibrations.

The three calibrations primarily differ in shape and positioning of the critical state line (CSL) from low stresses (most important for simulating the DSS data) to high stresses (most important for simulating cone penetration) because of the different values assigned to parameter ϕ'_{mr}, m_{s1}, and p_{ϕ} (Table 2). These differences are illustrated in Fig. 10 which shows the calibrations' CSLs (for triaxial compression loading) and 1-D compression curves. All three calibrations have the same 1-D and isotropic LCCs as shown in Fig. 10a, and accurately capture the measured 1-D compression behavior as shown in Fig. 10b. Note that the CSL predicted by the MIT-S1 model is slightly dependent on the loading condition, which is why the triaxial compression loading condition must be specified when referring to these CSLs.

The three calibrations represent tradeoffs between prioritizing: (1) the ability to simulate the monotonic undrained DSS test results, and (2) maintaining a reasonable spacing between the CSL and LCC at high confining stresses. The measured and simulated monotonic undrained DSS responses for $D_R \approx 30\%$ and 75% and σ'_{vc} = 100, 200, and 800 kPa are shown in Fig. 13; these test conditions only constrain the location of the CSL for p' values between about 50 and 2,000 kPa (i.e., the upper flatter portions of the CSLs in Fig. 10a). However, the simulations of cone penetration are controlled by the position of the CSL at higher stresses (e.g., p' of 2 to 20 MPa), which includes the steeper portions of the CSLs in Fig. 10a. The steeper portions of the CSLs are

approximately parallel to the LCC, and thus their position can be described by the ratio of the p' value on the isotropic LCC to the p' value on the triaxial compression CSL for a given void ratio (i.e., $p'_{ISO-LCC}/p'_{TC-CSL}$).

Calibration 1 prioritized simulating the monotonic undrained DSS test results, which required a slightly steeper CSL at low stresses and a $p'_{ISO-LCC}/p'_{TC-CSL} \approx 6$ near void ratios of 0.5-0.6 (corresponding to p' of 10-20 MPa on the CSL), as shown in Fig. 10a. This calibration produced the best overall agreement with the measured DSS responses (Fig. 13), but the $p'_{ISO-LCC}/p'_{TC-CSL} \approx 6$ is unreasonably large and is later shown to result in under-estimation of cone penetration resistances. In this regard, the other sets of calibration parameters can be selected to further improve agreement with the DSS test results, but they result in even larger values for $p'_{ISO-LCC}/p'_{TC-CSL}$ and poorer agreement with cone penetration resistances.

Calibration 2 anchors the CSL position closer to the LCC than Calibration 1 such that $p'_{ISO-LCC}/p'_{TC-CSL} \approx 3$ near void ratios of 0.5-0.6, which is consistent with LCC-CSL spacing in clays and cohesionless soils at high stresses (Lade and Yamamuro 1996). At very low stresses ($p' \approx 1$ kPa), the CSL is anchored to the Ottawa sand e_{max}. This calibration produced the poorest agreement with the DSS test results (Fig. 13), but is considered more reasonable for simulating responses at the higher stresses that develop during cone penetration.

Calibration 3 anchors the CSL at $p'_{ISO-LCC}/p'_{TC-CSL} \approx 3$ at higher stresses similar to Calibration 2, but lowers the CSL at lower stresses to improve the simulations of the DSS test results. This calibration produced the flattest upper portion of the CSL which impeded the ability to simulate the observed effect of confining stress on DSS responses. Nonetheless, this calibration produced an intermediate level of overall agreement with the DSS test results (Fig. 13), while retaining the desired LCC-CSL spacing at higher stresses (Fig. 10a).

$q_c - D_R$ Relationship

Cone penetration simulations using the three MIT-S1 calibrations were used to develop $q_{c1} - D_R$ relationships (where q_{c1} is the value of q_c when σ'_{vo} = 1 atm), which could then be compared to the empirical correlations and centrifuge test measurements. The simulated penetration resistances at σ'_{vo} = 100 kPa for D_R = 20% to 100% are plotted in Fig. 14a. At higher D_R, the simulated q_{c1} are lowest for Calibration 1 and similar for Calibrations 2 and 3, which is consistent with the relative positions of their CSL at lower void ratios (Fig. 10a). At lower D_R, the simulated q_{c1} are similar for Calibrations 1 and 3 and greater for Calibration 2, which is consistent with the relative positions of their CSL at higher void ratios (Fig. 10a). Empirical $q_{c1} - D_R$ correlations from Jamiolkowski et al. (2003) and from work by Salgado et al. (1997a,b) are shown in Fig. 14b. The work by Salgado et al. (1997a,b) involved numerical simulations calibrated to a set of calibration chamber test results, and included simulation results for lower-bound and upper-bound property sets. Idriss and Boulanger (2008) provided a regression equation that approximated the Salgado et al. (1997a,b) simulation results with a fitting parameter C_{dq} that ranged from 0.64 to 1.55. The simulation results using Calibration 3 (Fig. 14a) are reasonably consistent with the empirical correlations by Salgado et al. (1997a,b) for C_{dq} = 0.9. The simulation results using Calibrations 1 and 2 generally fall within the bounds of the Salgado et al. (1997a,b) correlation with C_{dq} = 0.64 to 1.55. The results of the centrifuge in-flight cone penetration tests on virgin models (before any shaking events) are shown in Fig. 14c. The present simulation results using Calibration 3 (Fig. 14a) show the best agreement with the centrifuge data (Fig. 14c), although the simulated q_{c1} are greater than those measured in the centrifuge for $D_R \approx 25 - 43\%$. The $q_c - D_R$ relationships in Figs. 14a and 14c were fit with a consistent equation to the Salgado et al. (1997a,b) relationship:

$$q_{c1} = C_{dq}\left(\frac{D_R + A}{B}\right)^{1/0.264} \quad (2)$$

where A and B are fitting parameters and C_{dq} is 1 for the $q_c - D_R$ relationships in Figs. 14a and 14c.

The influence of the CSL's position on q_c is further illustrated in Fig. 15 showing the $e - p'$ path of soil elements directly in the path of the penetrating cone, as computed using the three MIT-S1 calibrations. The soil begins at the initial in-situ stress condition of σ'_v = 100 kPa, $K_o = 0.5$, and D_R = 60% near the bottom boundary, then dilates to be approximately on the triaxial compression CSL as it nears the penetrating cone tip, and then slightly unloads as it moves around the cone shoulder. These paths illustrate that the steeper portion of the CSL most strongly influences the state of stress that develops near the cone tip and hence q_c.

Results of cone penetration simulations using Calibration 3 with D_R = 40%, 60%, and 80% and σ'_{vo} = 50, 100, 200, and 400 kPa are shown in Fig. 16. The relationship between q_c and σ'_{vo} can be approximated by a power law where σ'_{vo} is raised to a power m:

$$q_c = q_{c1}\left(\frac{\sigma'_{vo}}{P_a}\right)^m \quad (3)$$

The m values from the simulation results in Fig. 16 are 0.52, 0.42, and 0.40 for these D_R values, respectively. These are reasonably consistent with the Idriss and Boulanger (2008) relationship where m = 0.58, 0.47, and 0.37 were specified for D_R = 40%, 60%, and 80%, respectively.

Mechanistic Development of $CRR - q_{c1}$ Relationships

$CRR - q_{c1}$ relationships for Ottawa sand were developed with different approaches to synthesize data from laboratory tests, centrifuge tests, cone penetration simulations, and empirical

$q_{c1} - D_R$ relationships. The derived $CRR - q_{c1}$ relationships are compared to the Boulanger and Idriss (2016) case history-based correlation and centrifuge test data in Fig. 17.

The two $CRR - q_{c1}$ relationships in Fig. 17a were developed using the centrifuge test data. The relationship for $CRR - q_{c1}$ represented by the grey line in Fig. 17a was obtained by composing the $CRR - D_R$ relationship from the cyclic DSS tests (Fig. 5) with the $D_R - q_{c1}$ relationship from the in-flight cone penetration tests (Fig. 14c). The $CRR - q_{c1}$ relationship represented by the black line in Fig. 17a was developed directly with the centrifuge CRR and CSR values from inverse analyses of sensor array data for each shaking event and the in-flight cone penetration profiles shown in Fig. 8. The relationship fits through the points where liquefaction triggered while falling above most of the liquefaction not triggered points. These two $CRR - q_{c1}$ relationships are reasonably consistent with each other and with the case history-based correlation of Boulanger and Idriss (2016). The two derived relationships give slightly greater CRR values than the case history-based correlation for q_{c1N} values between 120 and 160, but these differences are not large.

The three $CRR - q_{c1}$ relationships in Fig. 17b were developed by composing the $CRR - D_R$ relationship from the cyclic DSS test data (Fig. 5) with the $D_R - q_{c1}$ relationships from the cone penetration simulations for the three different calibrations of MIT-S1 (Fig. 14a). The $CRR - q_{c1}$ relationship from Calibration 3 is reasonably consistent with the centrifuge data and the case history-based correlation, whereas the relationship for Calibration 2 is lower. The $CRR - q_{c1}$ relationship for Calibration 1 is well above the centrifuge data and case history-based correlation, which is consistent with its underestimation of cone penetration resistances (Figs. 14a and 14c).

The two $CRR - q_{c1}$ relationships in Fig. 17c were developed by composing the $CRR - D_R$ relationship from the cyclic DSS test (Fig. 5) with the empirical $D_R - q_{c1}$ relationships for clean silica sands by Jamiolkowski et al. (2003) and Salgado et al. (1997a,b) shown previously in Fig. 14b. The $CRR - q_{c1}$ relationship using the Salgado et al. (1997a,b) relationship with C_{dq} = 0.9 is reasonably consistent with the centrifuge data and the case history-based correlation, whereas the curve obtained using the Jamiolkowski et al. (2003) relationship is significantly lower for denser conditions.

Discussion

The approaches used herein to develop $CRR - q_{c1}$ relationships were able to produce results that are reasonably consistent with case history-based correlations for clean sands, as shown in Fig. 17, while also illustrating challenges that led to discrepancies with the correlations in some situations. The in-flight cone penetration tests were a vital component for all approaches, whether the measured q_c values were used directly or used to calibrate a soil constitutive model for numerical cone penetration simulations. The numerical cone penetration simulations were valuable for covering a broader range of soil density and confining stress conditions than can reasonably be measured in centrifuge tests, but validation of the computed q_c values against physical measurements was essential before the results could be used with confidence. The determination of CRR values by laboratory DSS testing provided a means for covering a broad range of soil density and confining stress conditions, whereas the determination of CRR values from inverse analyses of the dynamic centrifuge test data had the advantage that they came from the same model in which cone penetration measurements were obtained. A disadvantage of determining CRR values from dynamic centrifuge test data was the greater uncertainty in CRR values, especially for

denser conditions, which arise from complexities involved in interpreting nonlinear dynamic site responses involving liquefaction (e.g., Darby et al. 2019a,b). Developing $CRR - q_{c1}$ relationships through different approaches was advantageous since (1) it led to increased confidence when the various results were consistent, and (2) it led to insights and improvements when the results showed notable discrepancies (e.g., comparing the $CRR - q_{c1}$ relationships from the three MIT-S1 calibration simulations).

Although the mechanistically derived $CRR - q_{c1}$ relationships were developed with a clean, uniform, sand, the results showed an encouraging amount of agreement with case history-based correlations where many other environmental factors can influence the liquefaction resistance of in-situ sands (e.g., age, cementation, over-consolidation). This observation supports the implicit assumption embedded in current engineering practice that such factors may have similar effects on both CRR and q_{c1}, such that the $CRR - q_{c1}$ correlation is not strongly affected (e.g., Seed et al. 1979), at least for the range of conditions represented in the case history database. In addition, the results of the present study provide support for case history-based correlations at higher q_{c1} and CSR values where case history data are relatively limited.

A primary benefit of the present study was demonstrating that the framework outlined in Fig. 1 provides reasonable options for developing $CRR - q_{c1}$ relationships for a range of challenging soil types that are not well represented in case history databases. For example, practice routinely evaluates cyclic strengths and potential ground deformations for a range of tailings materials, waste materials (e.g., flyash), carbonate soils, intermediate soils (e.g., clayey sands, sandy silts), or organic soils for which case history-based correlations are not available. Furthermore, many of these soils exhibit strength and stress-strain characteristics that do not fit within traditional frameworks for describing sand-like or clay-like soil properties, therefore it is

essential that data for both CRR and q_c be obtained across a broad range of conditions from specimens and models prepared by similar means. For these reasons, systematic programs of dynamic centrifuge model testing with in-flight cone penetration testing, numerical simulations of cone penetration, and laboratory testing to determine monotonic and cyclic strengths, provide a strong basis to address persistent knowledge gaps regarding the potential seismic loading responses of various challenging soil types.

Conclusions

A number of mechanistic approaches for developing liquefaction triggering relationships from cone penetration test measurements were presented and evaluated with an application to Ottawa sand. Cyclic direct simple shear tests on Ottawa sand characterized the relationship between cyclic resistance ratio (CRR) and relative density (D_R). Dynamic centrifuge model tests provided in-flight measurements of cone tip resistance (q_c) and CRR values from inverse analyses of sensor array data over multiple shaking events. Penetration simulations with three different MIT-S1 constitutive model calibrations for Ottawa sand illustrated the role of critical state line shape and position on q_c values. Different approaches to combining the above information were able to produce $CRR - q_{c1N}$ relationships that are reasonably consistent with case history-based correlations for clean sands, while also illustrating challenges that led to greater discrepancies in some situations. The results of this study suggest that a combination of mechanistic approaches, as illustrated in Fig. 1, provides a reasonable option for developing $CRR - q_{c1}$ relationships for a range of challenging soil types that are not well represented in case history databases.

Acknowledgments

Funding for this research was provided by the National Science Foundation (award CMMI-1300518) and the California Department of Water Resources (contract 4600009751). Funding for the Natural Hazards Engineering Research Infrastructure (NHERI) centrifuge facility at UC Davis was provided by the National Science Foundation (award CMMI-1520581). Part of the funding for the laboratory testing was provided by COLCIENCIAS call 529 of 2011 doctoral loan-scholarship program. Any opinions, findings, and conclusions or recommendations expressed in this material are those of the authors and do not necessarily reflect the views of either agency.

References

Been, K., and Jeffries M.G. (1985). "A state parameter for sands." *Geotechnique*, 16, 338-357.

Boulanger, R. W., and Idriss, I. M. (2016). "CPT-based liquefaction triggering procedure." Journal of Geotechnical and Geoenvironmental Engineering, ASCE, 142(2), 04015065, 10.1061/(ASCE)GT.1943-5606.0001388.

Boulanger, R. W., and Idriss, I. M. (2014) "CPT and SPT based liquefaction triggering procedures." Geotechnical Engineering Research Report No. UCD/CGM-14/01.

Carlton, B.D., and Pestana, J.M. (2016). "A unified model for estimating the in-situ small strain shear modulus of clays, silts, sands, and gravels." *Soil Dyn. Earthq. Eng.,* 88, 345-355.

Carraro, J. A. H., Bandini, P., and Salgado, R. (2003). "Liquefaction resistance of clean and nonplastic silty sands based on cone penetration resistance." *Journal of Geotechnical and Geoenvironmental Engineering,* 129(11), 965-976. 10.1061/(ASCE)1090-0241(2003)129:11(965).

Colella, P. (1990). "Multidimensional upwind methods for hyperbolic conservation laws." *J. of Comput. Phys.*, 87, 171-200.

Darby, K.M., Bronner, J.D., Parra Bastidas, A.M., Boulanger, R.W., and DeJong, J.T. (2016). "Effect of shaking history on the cone penetration resistance and cyclic strength of saturated sand." *Proc. of the Geotechnical and Structural Engineering Congress 2016,* Phoenix, Arizona,1460-1471.

Darby, K. M., Boulanger, R. W., and DeJong, J. T. (2017). "Effect of multiple shaking events on cone penetration resistances in saturated sand." *Proc., Performance-based Design in Earthquake*

Geotechnical Engineering, PBD-III Vancouver, M. Taiebat et al., eds., ISSMGE Technical Committee TC203, paper 534.

Darby, K. M., Boulanger, R. W., DeJong, J. T., and Bronner, J. D. (2019a). "Progressive changes in liquefaction and cone penetration resistance across multiple shaking events in centrifuge tests." *Journal of Geotechnical and Geoenvironmental Engineering,* 140(3): 04018112, 10.1061/(ASCE)GT.1943-5606.0001995.

Darby, K. M., Boulanger, R. W., and DeJong, J. T. (2019b). "Effect of partial drainage on cyclic strengths of saturated sands in dynamic centrifuge tests." *Journal of Geotechnical and Geoenvironmental Engineering,* in press.

Darendelli, M. B. (2001). "Development of a new family of normalized modulus reduction and material damping curves." PhD Thesis, Department of Civil, Architectural and Environmental Engineering, The University of Texas at Austin.

Idriss, I. M., and Boulanger, R. W. (2008). Soil liquefaction during earthquakes. Monograph MNO-12, *Earthquake Engineering Research Institute*, Oakland, CA.

Itasca (2016). FLAC Version 8.0. Itasca Consulting Group Inc., Minneapolis, Minnesota.

Jaeger, R. A. (2012). "Numerical and experimental study on cone penetration in sands and intermediate soils." PhD Thesis, Department of Civil and Environmental Engineering, University of California, Davis.

Jaky, J. (1949). "Pressure in soils." *Proceedings 2nd International Conference on Soil Mechanics and Foundation Engineering*, 103-107.

Jamiolkowski, M., Lo Presti, D. C. F., and Manassero, M. (2003). "Evaluation of relative density and shear strength of sands from CPT and DMT." *Soil Behavior and Soft Ground Construction,* 201-238. doi.org/10.1061/40659(2003)7

Kamai, R., and Boulanger, R.W. (2010). "Characterizing localization processes during liquefaction using inverse analyses of instrumentation arrays." *Meso-Scale Shear Physics in Earthquake and Landslide Mechanics,* Y. H. Hatzor, J. Sulem, and I. Vardoulakis, eds., CRC Press, 219-238.

Kokusho, T., Tadashi, H., and Murahata, K. (2006). "Liquefaction strength of sands containing fines compared with cone resistance in triaxial specimens." *Geomechanics II: Testing, Modeling, and Simulation,* 356-373. 10.1061/40870(216)24.

Kulhawy, F.H., and Mayne, P.W. (1990). "Manual on estimating soil properties for foundation design. No. EPRI-EL-6800. Electric Power Research Inst., Palo Alto, CA (USA); Cornell Univ., Ithaca, NY (USA). Geotechnical Engineering Group, 1990.

Lade, P.V., and Yamamuro, J.A. (1996). "Undrained sand behavior in axisymmetric tests at high pressures." *Journal of Geotechnical Engineering,* 122(2), 120-129. 10.1061/(ASCE)0733-9410(1996)122:2(120), 120-129

Mitchell, J.K., and Tseng, D.J. (1990). "Assessment of liquefaction potential by cone penetration resistance." *Proc. HB Seed Memorial Symp.* Vol. 2.

Moug, D.M. (2017). "Axisymmetric cone penetration model for sands and clays." PhD Thesis, Department of Civil and Environmental Engineering, University of California, Davis.

Moug, D.M., Boulanger, R.W., DeJong, J.T., and Jaeger, R.A. (2019). "Axisymmetric cone penetration simulations in saturated clay." *Journal of Geotechnical and Geoenvironmental Engineering,*145(4), 10.1061/(ASCE)GT.1943-5606.0002024.

Moss, R.E.S., Seed, R.B., Kayen, R.E., Stewart, J.P., Youd, T.L., and Tokimatsu, K. (2003). "Field case histories for CPT-based in situ liquefaction potential evaluation." Geoengineering Research Report No. UCB/GE-2003/04.

Oztoprak, S. and Bolton, M.D. (2013). "Stiffness of sands through a laboratory test database." *Geotechnique*, 1, 54-70. http://dx.doi.org/10.1680/geot.10.P.078

Parra Bastidas, A M., (2016). "Ottawa F-65 sand characterization." PhD Thesis, Department of Civil and Environmental Engineering, University of California, Davis.

Parra Bastidas, A. M., Boulanger, R. W., Carey, T. J., and DeJong, J. T. (2016). "Ottawa F-65 Sand Data from Ana Maria Parra Bastidas" *NEEShub*, http://dx.doi.org/10.17603/DS2MW2R

Parra Bastidas, A.M., Boulanger, R.W., DeJong, J.T., and Price, A.B. (2017). "Effects of pre-strain history on the cyclic resistance of Ottawa F-65 sand." *Proc. 16th World Conf. on Earthquake Engineering,* Santiago, Chile, No. 1213.

Pestana, J.M., and Whittle, A.J. (1995). "Compression model for cohesionless soils." *Geotechnique,* 45(4), 611-631.

Pestana, J.M., and Whittle, A.J. (1999). "Formulation of a unified constitutive model for clays and sands." *Int. J. Numer. Anal. Meth. Geomech.,* 23, 1215-1243.

Pestana, J.M., Whittle, A.J., and Salvati, L.A. (2002). "Evaluation of a constitutive model for clays and sands: Part I – sand behaviour." *Int. J. Numer. Anal. Meth. Geomech.,* 26, 1097-1121.

Pestana, J.M., Whittle, A.J., and Gens, A. (2002). "Evaluation of a constitutive model for clays and sands: Part II – clay behaviour." *Int. J. Numer. Anal. Meth. Geomech.,* 26, 1123-1146.

Price, A. B. (2018). "Cyclic strength and cone penetration resistance for mixtures of silica silt and kaolin." PhD Thesis, Department of Civil and Environmental Engineering, University of California, Davis.

Robertson, P. K., and Campanella, R. G. (1985). "Liquefaction potential of sands using the CPT." *Journal of Geotechnical Engineering*, 111(3), 384-403. 10.1061/(ASCE)0733-9410(1985)111:3(384).

Robertson, P.K. and Wride, C.E. (1998). "Evaluating cyclic liquefaction potential using the cone penetration test." *Can. Geotech. J.,* 35(3), 442-459.

Salgado, R., Mitchell, J.K, Jamiolkowski, M. (1997). "Cavity expansion and penetration resistance in sand." *J. Geotech. Geoenviron. Eng.,* 10.1061/(ASCE)1090-0241(1997)123:4(233), 344-354.

Salgado, R., Boulanger, R.W., and Mitchell, J.K. (1997). "Lateral stress effects on CPT liquefaction resistance correlations." *J. Geotech. Geoenviron. Eng.,* 10.1061/(ASCE)1090-0241(1997)123:8(726), 726-735.

Seed, H. B. (1979). "Soil liquefaction and cyclic mobility evaluation for level ground during earthquakes." J. Geotechnical Eng. Div, ASCE 105(GT2), 201–255.

Seed, H. B., and De Alba, P. (1986). "Use of SPT and CPT tests for evaluating the liquefaction resistance of sands." *Use of in situ tests in geotechnical engineering.* ASCE, 281-302.

Seed, H. B., and Idriss, I M. (1970). "Soil moduli and damping factors for dynamic response analysis." Report No. EERC 70-10, University of California, Berkeley.

Seed, H. B., Idriss, I. M., Makdisi, F., and Banerjee, N. (1975). "Representation of irregular stress time histories by equivalent uniform stress series in liquefaction analyses." Report No. EERC 75-29, Earthquake Engineering Research Center, University of California, Berkeley.

Uesugi, M., and Kishida, H. (1986). "Frictional resistance at yield between dry sand and mild steel." *Soils and Found.,* 26(4), 139-149.

Vaid, P., and Sasitharan, S. (1992) "The strength and dilatancy of sand." *Can. Geotech. J.,* 29(3): 522-526.

Youd, T.L., Idriss, I.M., Andrus, R.D., Arango, I., Castro, G., Christian, J.T., Dobry, R., Finn, W.D., Harder, L.F., Hynes, M.E., Ishihara, K., Koester, J.P., Liao, S.S.C., Marcuson, W.F., Martin, G.R., Mitchell J.K., Moriwaki, Y., Power, M.S., Robertson, P.K., Seed, R.B., and Stokoe, K.H. (2001). "Liquefaction resistance of soils: summary report from the 1996 NCEER and 1998 NCEER/NSF workshops on evaluation of liquefaction resistance of soil. *J. Geotechnical and Geoenvironmental Eng.,* 10.1061/(ASCE)1090-0241(2001)127:10(817), 817-833.

Ziotopoulou, K., Montgomery, J., Parra Bastidas, A. M., and Morales, B. (2018). "Cyclic strength of Ottawa F-65 sand: laboratory testing and constitutive model calibration." *Proc. Geotechnical Earthquake Engineering and Soil Dynamics V,* Geotechnical Special Publication 293. S. J. Brandenberg and M. T. Manzari, eds., ASCE, 180-189.

Table 1. Ottawa sand index properties

Index property	Value
Fines Content	0.17%
D_{10}	0.14 mm
D_{50}	0.20 mm
Coefficient of Curvature, C_c	0.96
Coefficient of Uniformity, C_u	1.61
e_{min}	0.507
e_{max}	0.833
Specific Gravity of Solids, G_s	2.65
Silica Content	99.5%

Table 2. MIT-S1 calibrations for Ottawa sand

MIT-S1 Parameter	Parameter Description	Calibration 1	2	3
ρ_c	Slope of limiting compression curve in $\log(e) - \log(p')$ space		0.49	
$\sigma'_{v,ref}/p_{atm}$	Reference p' at $e = 1$ on the 1-D limiting compression curve		129.0	
θ	Controls transition to limiting compression curve ($\theta = 0$ for clays)		0.25	
D	Characterizes slope of unloading curve		0.0	
r	Characterizes shape of unloading curve		0.0	
K_{0NC}	Lateral earth pressure coefficient at normally consolidated conditions		0.50	
μ'_o	Small strain Poisson's ratio		0.23	
ω	Controls non-linearity in Poisson's ratio		1.0	
C_b	Controls small strain elastic moduli.		899.0	
ϕ'_{cs}	Critical state friction angle		30.0	
ϕ'_{mr}	Peak friction angle at $e = 1$	21.25	19.965	18.2045
p_ϕ	Controls variation of peak friction angle with void ratio ($p_\phi = 0$ for clays)	2.50	2.608	2.608
m_{s1}[a]	Controls shape of yield and bounding surfaces	0.35	0.60	0.67
ω_s	Controls non-linearity of elastic moduli in shear		8.0	
ψ	Controls rate of evolution of the yield surface anisotropy		60.0	
h	Controls plastic strain magnitude when over consolidation ratio > 1		2.0	

[a]parameter is represented by m in Pestana and Whittle (1999, 2002a,b), Jaeger (2012) and Moug (2017, 2019)

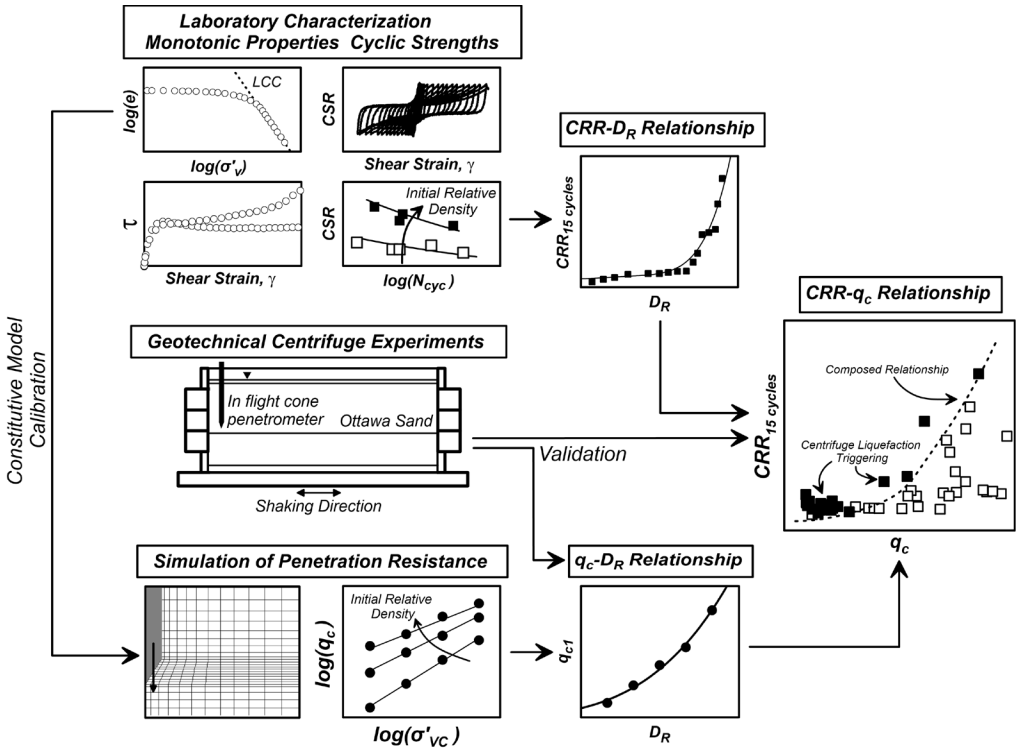

Fig. 1. Mechanistic approaches for developing alternate $CRR - q_c$ relationships from laboratory, centrifuge, and numerical simulation data

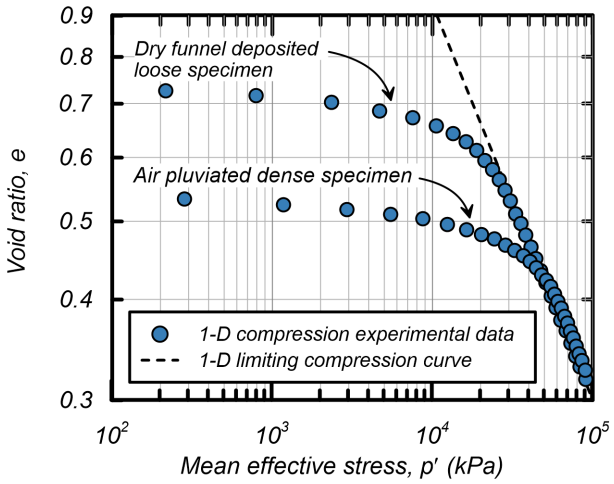

Fig. 2. Results from 1-D high stress compression tests on Ottawa sand

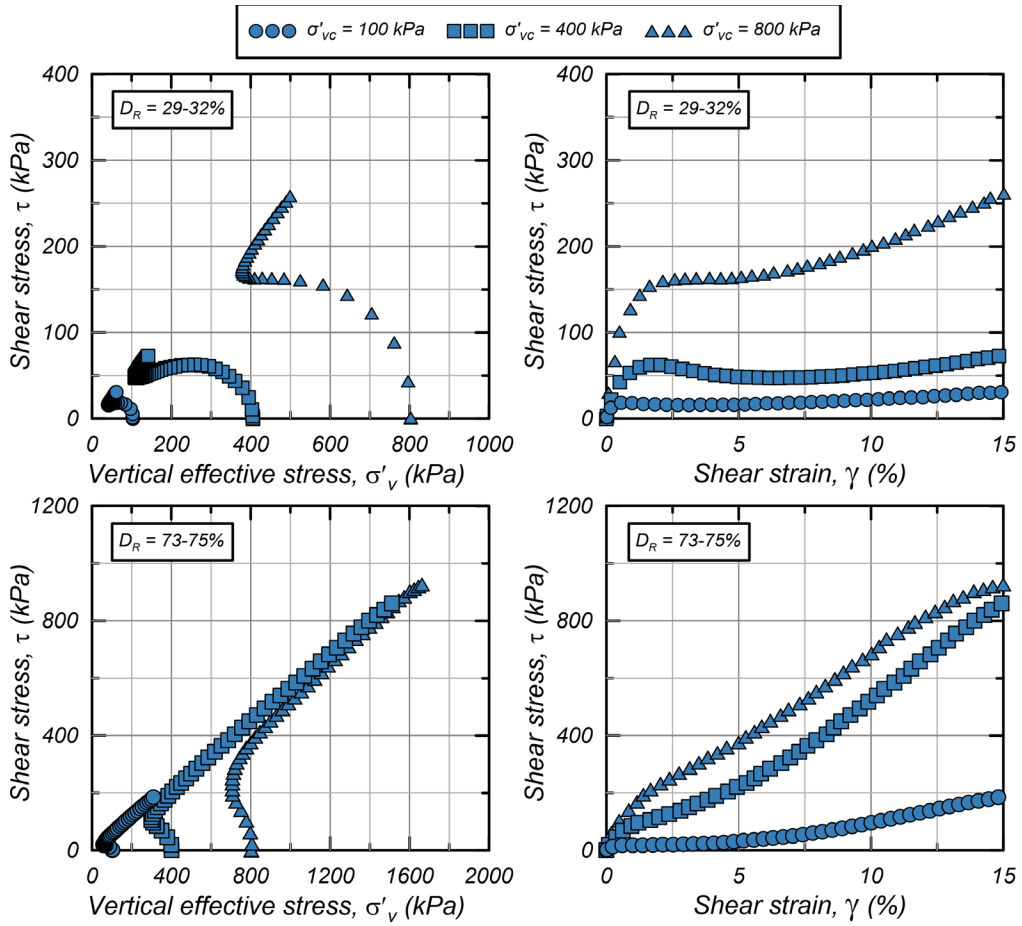

Fig. 3. Results from undrained monotonic direct simple shear tests on D_R=30% and D_R=75% on Ottawa sand

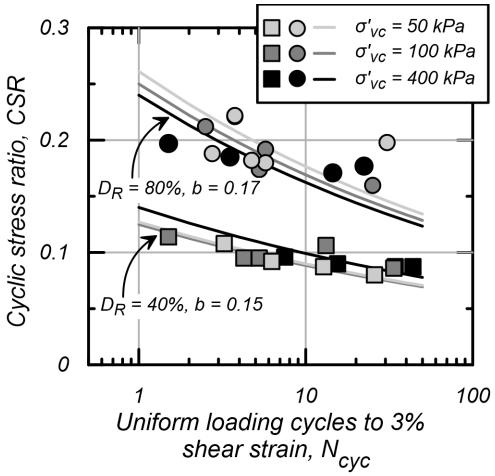

Fig. 4. *CRR* vs. number of number of uniform loading cycles from cyclic DSS tests on Ottawa sand (after Parra Bastidas et al. 2017)

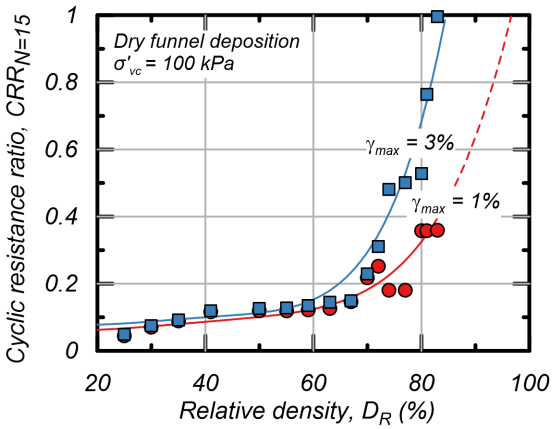

Fig. 5. Progression of CRR with increasing D_R for cyclic DSS tests with multiple loading and reconsolidation stages

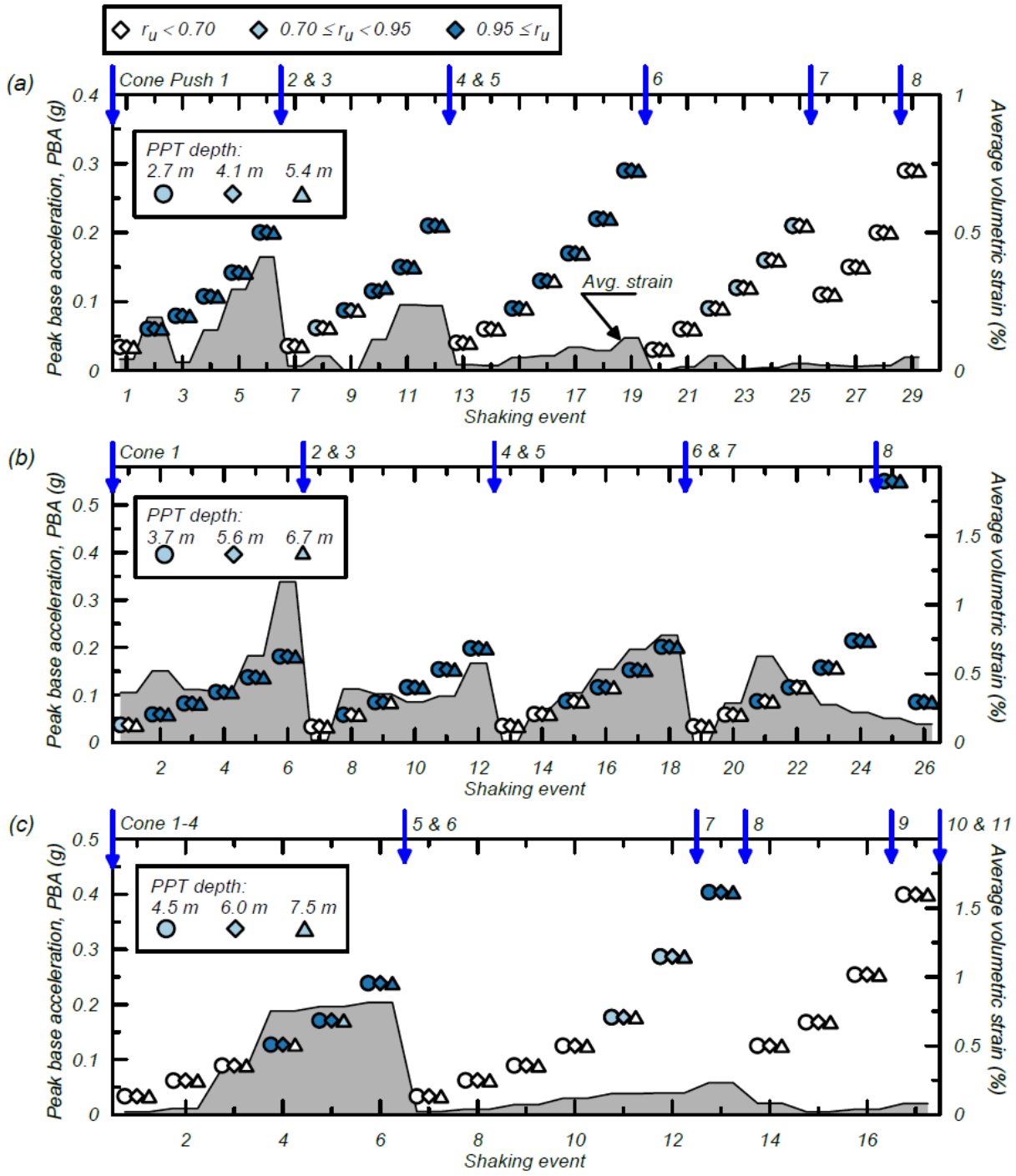

Fig. 6. Sequence of repeated shaking events and cone penetration tests for geotechnical centrifuge models: a) KMD01, b) KMD02, and c) KMD03

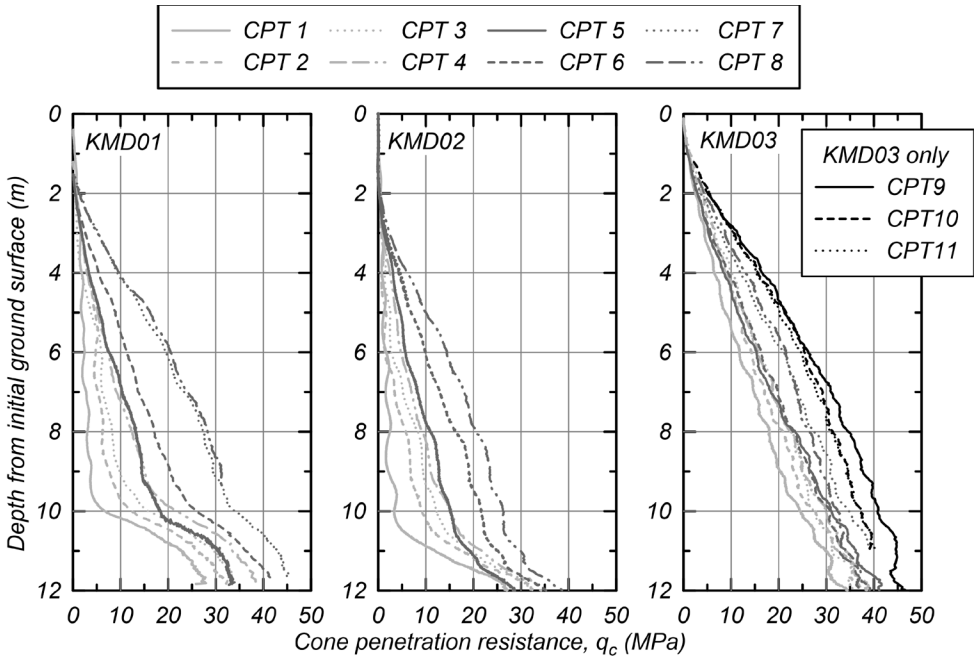

Fig. 7. Cone penetration profiles in geotechnical centrifuge models of Ottawa sand showing increases of measured q_c with repeated shaking events

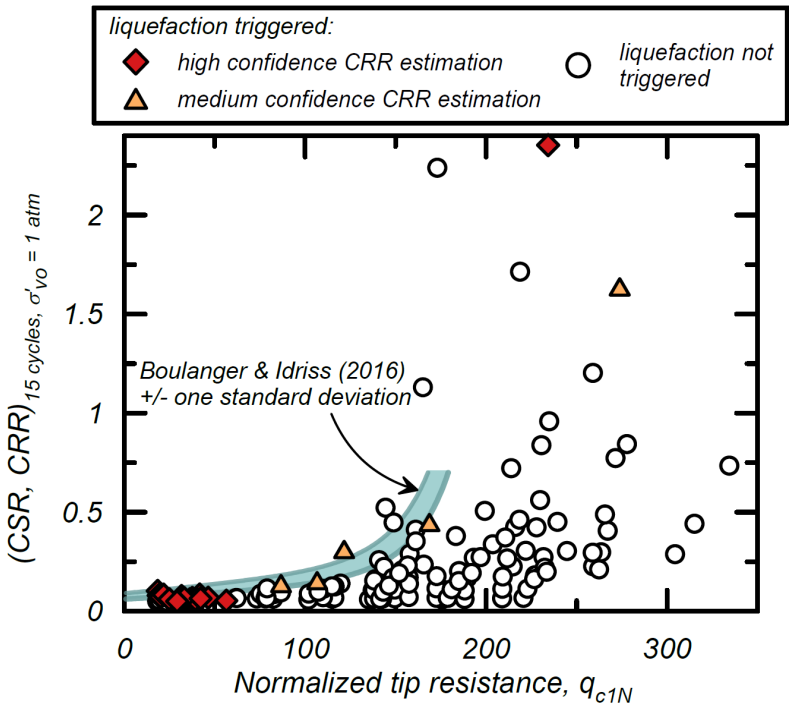

Fig. 8. CRR vs. q_{c1} liquefaction triggering or no triggering points from KMD centrifuge experiments

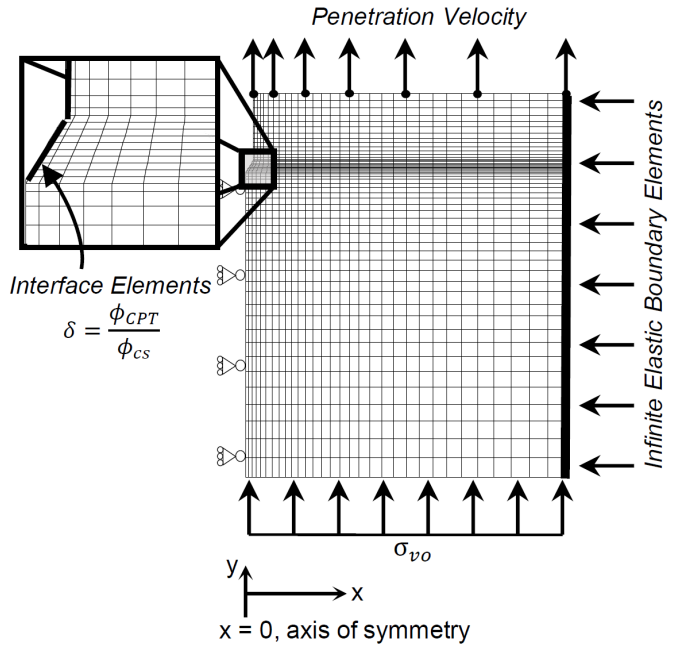

Fig. 9. Geometry and boundary conditions of the numerical cone penetration model in FLAC

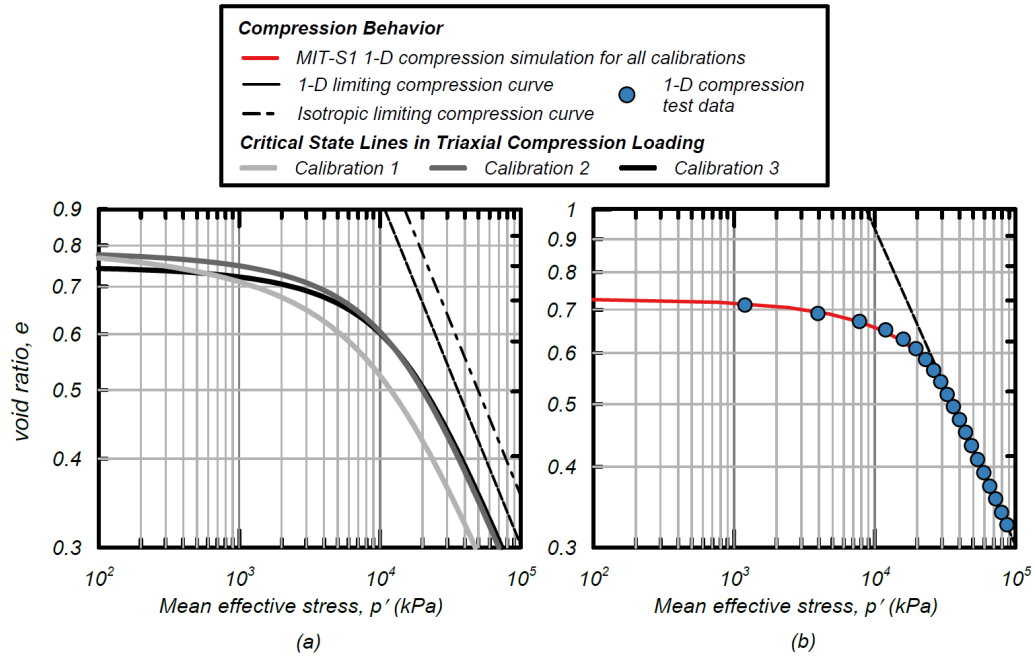

Fig. 10. a) Position of triaxial compression critical state lines and limiting compression curves for the three MIT-S1 Ottawa sand calibrations, and b) simulated and measured 1-D compression behavior

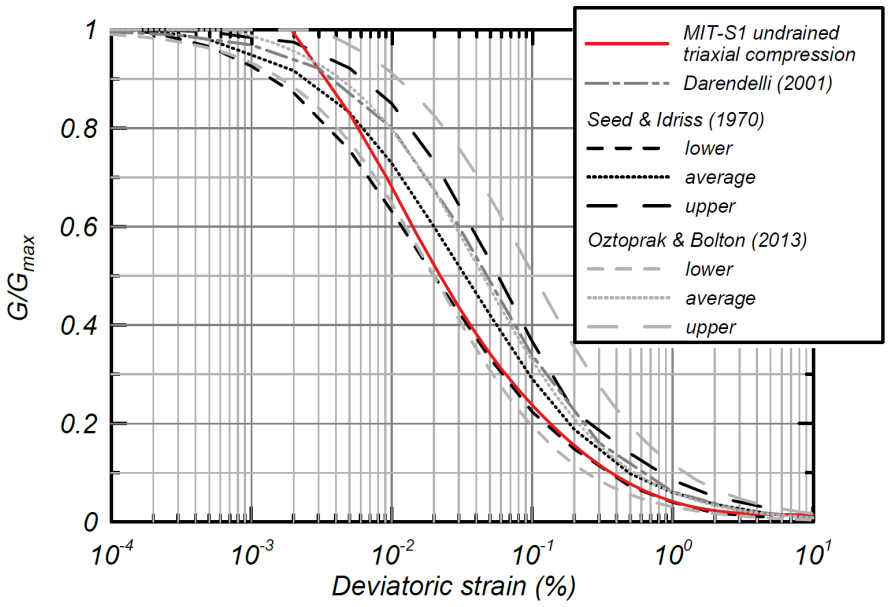

Fig. 11. Shear modulus degradation of MIT-S1 Ottawa sand calibrations compared to relationships by Darendelli (2001), Seed and Idriss (1970), and Oztoprak and Bolton (2013)

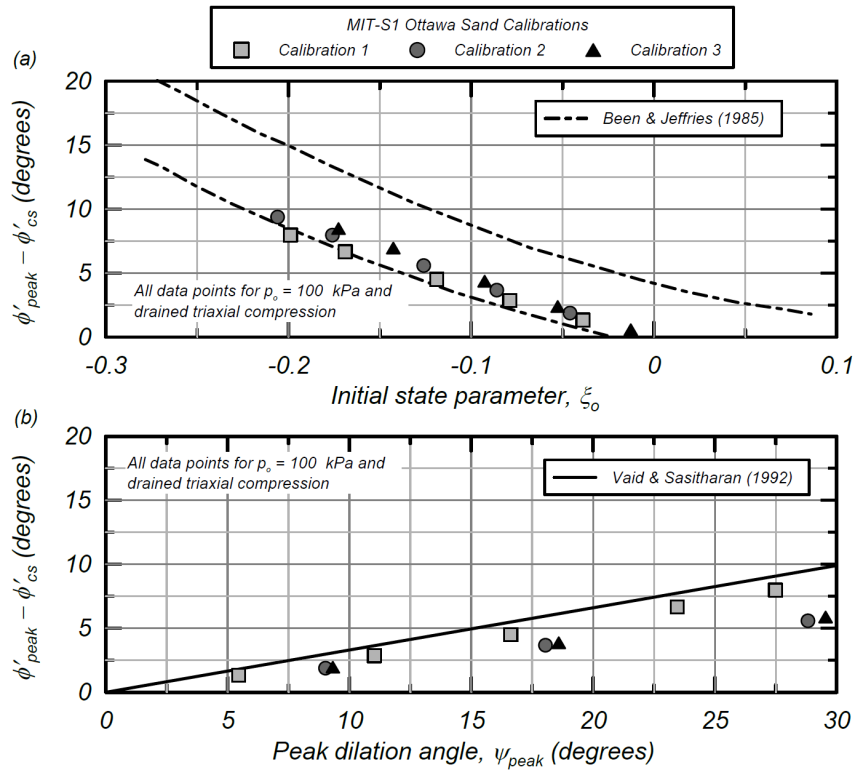

Fig. 12. Strength dilatancy for MIT-S1 Ottawa sand simulations in drained triaxial compression related to (a) initial soil state parameter and compared to Been and Jeffries (1985) and (b) peak soil dilation angle and compared to Vaid & Sasitharan (1992)

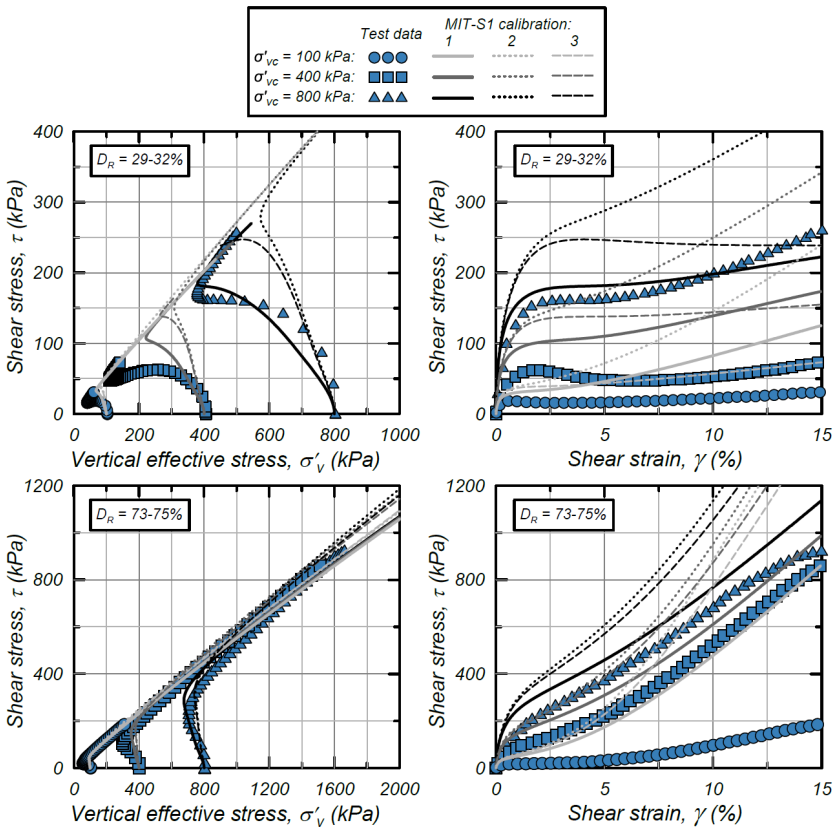

Fig. 13. Simulated MIT-S1 single element undrained DSS responses for three Ottawa sand calibrations

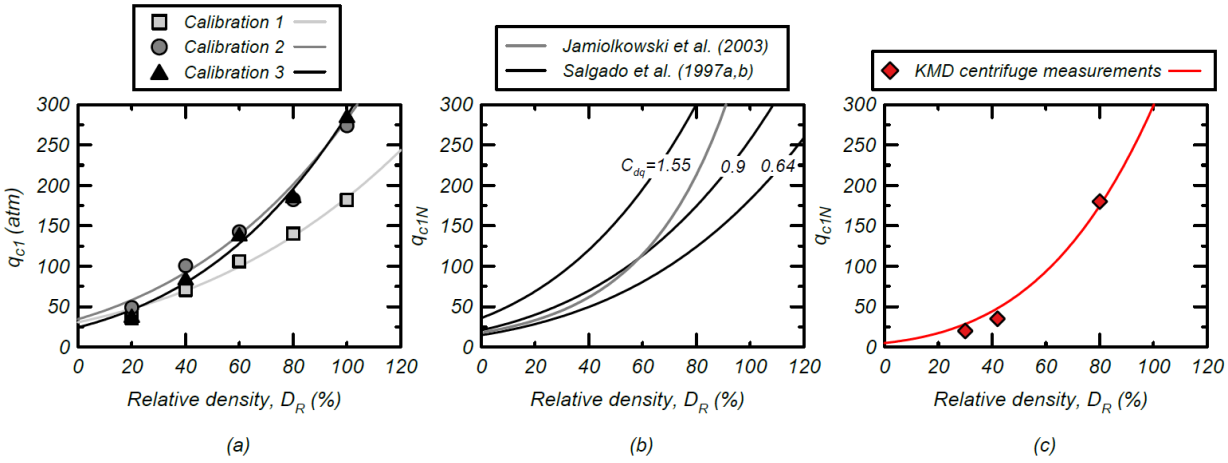

Fig. 14. (a) simulated cone penetration $q_{c1} - D_R$ points with interpolated relationship, (b) empirical $q_{c1N} - D_R$ relationships for clean sand, and (c) in-flight cone penetration $q_{c1} - D_R$ measurements with interpolated relationship

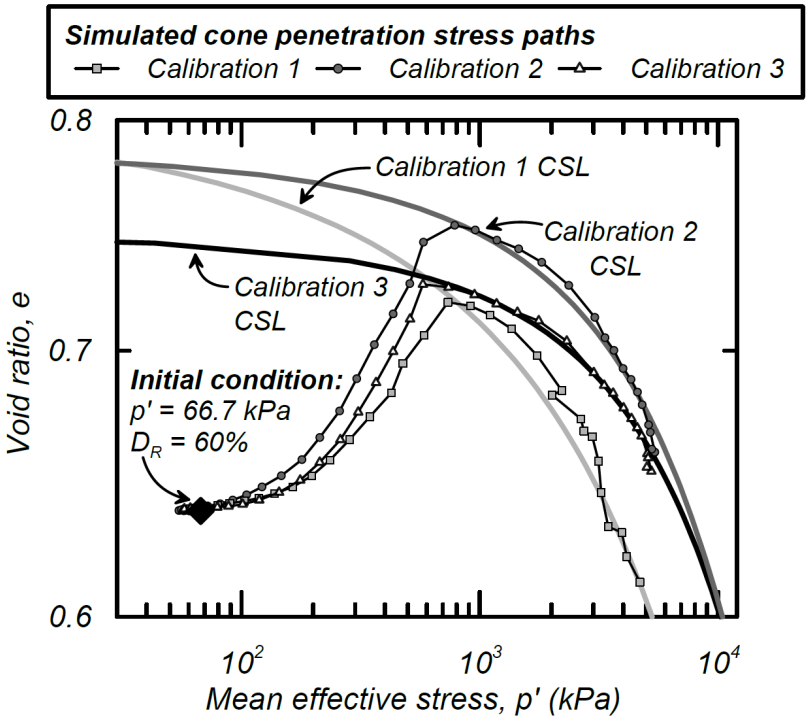

Fig. 15. Simulated $e - p'$ paths from in-situ conditions to the cone face

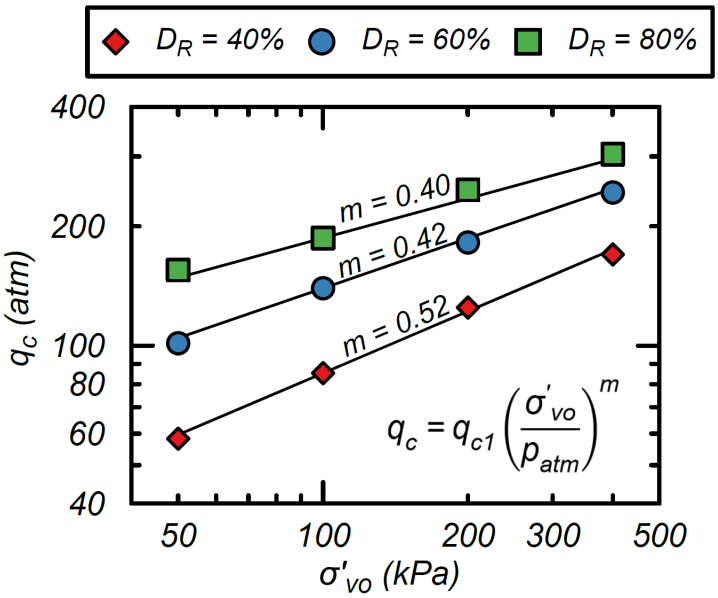

Fig. 16. Stress normalization relationship for simulated cone penetration with Ottawa sand Calibration 3

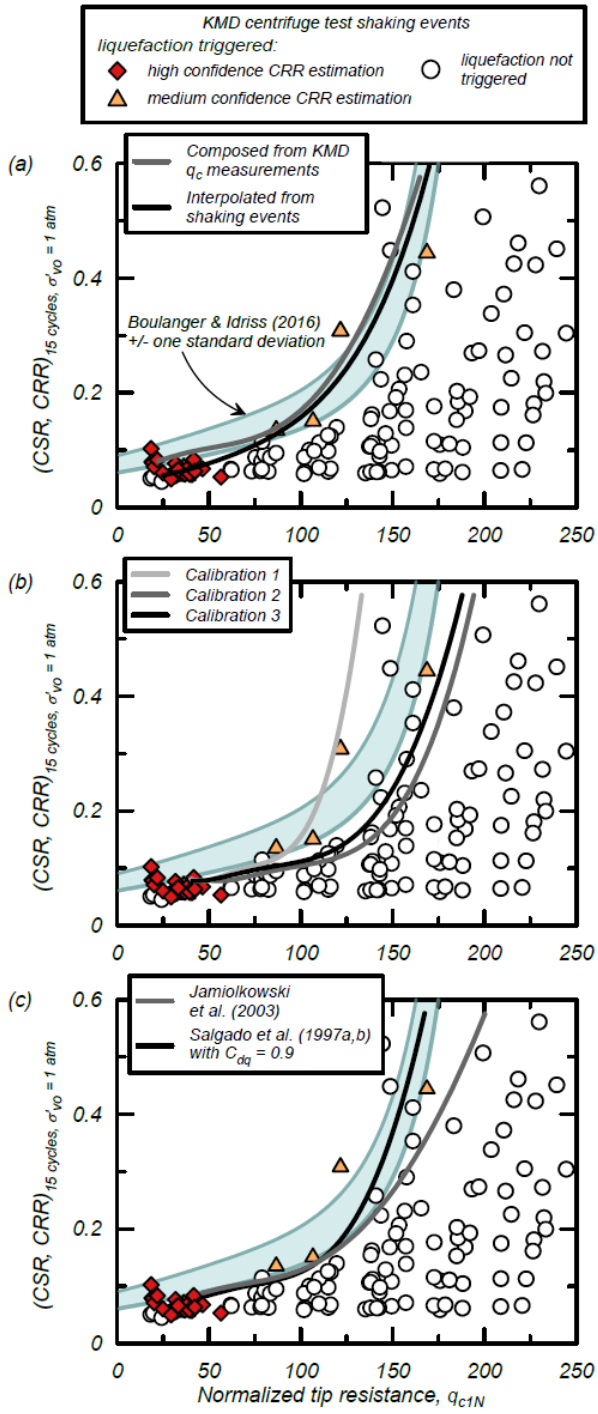

Fig. 17. $CRR - q_{c1N}$ relationships developed from: (a) centrifuge data directly or composing the laboratory $CRR - D_R$ relationship with the $D_R - q_{c1N}$ relationship from in-flight cone penetration profiles, (b) composing the laboratory $CRR - D_R$ relationship with $D_R - q_{c1N}$ relationships from cone penetration simulations, and (c) composing the laboratory $CRR - D_R$ relationship with empirical $D_R - q_{c1N}$ relationships